



CHORUS

This is the accepted manuscript made available via CHORUS. The article has been published as:

Series of phase transitions in cesium azide under high pressure studied by in situ x-ray diffraction

Dongbin Hou, Fuxiang Zhang, Cheng Ji, Trevor Hannon, Hongyang Zhu, Jianzhe Wu, and Yanzhang Ma

Phys. Rev. B **84**, 064127 — Published 30 August 2011

DOI: [10.1103/PhysRevB.84.064127](https://doi.org/10.1103/PhysRevB.84.064127)

**Series of phase transitions in cesium azide under high pressure
studied by in situ x-ray diffraction**

Dongbin Hou¹, Fuxiang Zhang², Cheng Ji¹, Trevor Hannon¹, Hongyang Zhu¹, Jianzhe
Wu¹, Yanzhang Ma*¹

¹*Department of Mechanical Engineering, Texas Tech University, Lubbock, Texas 79409, USA*

²*Department of Geological Sciences, University of Michigan, Ann Arbor, MI 48109-1005, USA*

**Corresponding author: Department of Mechanical Engineering, Texas Tech University, Lubbock, Texas*

79409, USA. Tel.: +1 806 742 3563; fax: +1 806 742 3540.

E-mail address: y.ma@ttu.edu

ABSTRACT

In situ X-ray diffraction measurements of cesium azide (CsN₃) were performed at high pressures up to 55.4 GPa at room temperature. Three phase transitions were revealed as follows: tetragonal (*I4/mcm*, Phase II) → monoclinic (*C2/m*, Phase III) → monoclinic (*P2₁/m* or *P2₁*, Phase IV) → triclinic (*P1* or *P $\bar{1}$* , Phase V), at 0.5 GPa, 4.4 GPa, and 15.4 GPa, respectively. During the II-III phase transition, CsN₃ keeps its layered structure; and the azide anions rotate obviously. The compressibility of Phase II is dominated by the repulsions between azide anions. The deformation of unit cell is isotropic in Phase II and IV, and anisotropic in Phase III. With increasing pressures, the monoclinic angle increases in Phase III and then becomes stable in Phase IV. The bulk moduli of Phase II, III, IV, and V are determined to be 18 ± 4 GPa, 20 ± 1 GPa, 27 ± 1 GPa and 34 ± 1 GPa, respectively. The ionic character of alkali azides is found to play a key role in their pressure-induced phase transitions.

I. INTRODUCTION

Inorganic azides are important materials¹⁻³ because of both their practical and theoretical applications. Practically, they are widely applied as explosives and pure nitrogen gas sources⁴⁻⁶; theoretically, they are simple systems that can be used in modeling the interatomic forces to study both the structure and the dynamics in various phases under different conditions⁷⁻⁹.

Alkali azides, a comparably stable species among inorganic azides, exhibits a variety of phase transitions stimulated by either temperature or pressure⁹⁻²⁰. During these phases, the behavior of the azide anions N_3^- is noticeable. In the temperature-induced phase transitions of both rubidium azide (RbN_3) and cesium azide (CsN_3), a fluctuation of the orientation of N_3^- anions was shown¹¹⁻¹³. In both the pressure-¹⁰ and temperature-induced¹⁸⁻²⁰ phase transition of sodium azide (NaN_3), a tilting of N_3^- anions also exhibits. Recently, the high-pressure effect on alkali azides has become a promising topic because of their application as a precursor to synthesize a high energetic density material of polymeric (non-molecular) form of nitrogen (N_2). A polymeric nitrogen phase under high pressure was first predicted early in 1985²¹. Then it was investigated with optical and electrical methods in 2000²² and 2001²³, respectively. A single-bonded cubic gauche form of N_2 was successfully synthesized in 2004²⁴ and 2007²⁵. Simultaneously, the N_3^- anions of NaN_3 at high pressure were also observed to transform to polymeric nitrogen nets in 2004¹⁴, and a cubic gauche structure in 2005¹⁵. The formation of a polymeric nitrogen network was also predicted on lithium azide (LiN_3) under high pressure²⁶. The mechanism of photolysis of NaN_3 under high pressure was also investigated to elucidate the potential to synthesize the high energetic density nitrogen structures²⁷. In this respect, an investigation of the high-pressure

behavior of CsN₃ would provide more insight into the pressure-induced rearrangement of N₃⁻ anions and phase transitions that might form the high energetic density material of polymeric nitrogen.

Under ambient conditions, CsN₃ crystallizes in a body centered tetragonal system with space group *I4/mcm*, and lattice parameters $a = 6.5412 \text{ \AA}$ and $c = 8.0908 \text{ \AA}$ (Phase II)²⁸. This particular tetragonal structure can be understood as a distorted cesium-chloride cubic structure (*Pm3m*) caused by the asphericity of the linear N₃⁻ anions (Fig. 1). At 151 °C and ambient pressure, CsN₃ undergoes a phase transition from the tetragonal Phase II to a cubic form in space group *Pm3m* (Phase I)¹¹. In contrast of Phase II, Phase I has randomly orientated N₃⁻ anions with respect to the edges of the cubic unit cell¹¹⁻¹³. At approximately 0.4 GPa and 25.7 °C Phase II transforms to a high-pressure form (Phase III) with a volume reduction of 4.2%⁹. A Raman study suggests that Phase III involves at least two crystallographically nonequivalent N₃⁻ ion sites¹², but the crystal structure of Phase III has not yet been determined.

The present paper reports the high-pressure phases and the compressibility of CsN₃ by means of a synchrotron X-ray diffraction measurement to 55.4 GPa in a diamond anvil cell.

II. EXPERIMENTAL

A symmetric diamond anvil cell with flat diamonds was used to generate high pressure in the experiments. The anvil was 400 μm in diameter. A rhenium gasket was used, with a hole of 150 μm in diameter and 60 μm in thickness, as sample chamber. The

99.99% CsN₃ powder was obtained from Sigma Aldrich (USA). A small flake of the sample with ~100 μm in diameter and ~30 μm in thickness was loaded into the sample chamber. Pressure was measured by the nonlinear shift of the wavelength of the ruby R1 line^{29, 30}. Neon gas, mineral oil and silicone oil were selected as pressure transmitting media in different experimental runs to rule out the possible contamination by products of the reaction of CsN₃ with the pressure media. *In situ* high-pressure angle-dispersive X-ray diffraction experiments at room temperature were performed at the beamline B2 of the Cornell High Energy Synchrotron Source (CHESS, Wilson Laboratory) at Cornell University and the beamline X17C in the National Synchrotron Light Source (NSLS) at Brookhaven National Laboratory. The experiments using mineral oil and neon as pressure media were performed in CHESS, and those using silicone oil were performed in NSLS. In the NSLS experiments, the sample was ground for a longer time than in CHESS to obtain more randomly oriented microcrystals of the sample. In CHESS, the X-ray had a wavelength of 0.4859 Å and was collimated to a beam size of 40 μm in diameter; the diffraction data were recorded on a MAR345 imaging plate. In NSLS, the X-ray beam had a wavelength of 0.4066 Å and was focused to a spot size of 27×21 μm²; the diffraction data were collected using a MAR CCD detector. The diffraction images were converted to 2θ versus intensity data plots using the FIT2D software³¹.

III. RESULTS AND DISCUSSION

The results reveal three pressure-induced phase transitions (II-III, III-IV, and IV-V) up to 55.4 GPa. For the first one, because the Phase II was observed at 0.4 GPa and the

Phase III was observed at 0.5 GPa, the onset of II-III transition lies in between 0.4 GPa and 0.5 GPa. It is in excellent agreement with the II-III boundary reported by Pistorius at 0.409 ± 0.042 GPa⁹, given the 0.1 GPa uncertainty in the ruby fluorescence pressure measurement system³². The second transition (III-IV) was observed by a coexistence of Phase III and IV at 4.4 GPa. And since only Phase III was observed at 3.8 GPa and only Phase IV was observed at 5.0 GPa, it can be inferred that the onset of the III-IV transition lies in between 3.8 and 4.4 GPa, and the completion between 4.4 and 5.0 GPa. The third transition (IV-V) is considerably sluggish. The coexistence of Phase IV and V was observed over the pressure range from 15.4 to 23.7 GPa. The onset of the IV-V transition lies in between 15.1 and 15.4 GPa, and the completion between 23.7 and 24.7 GPa. Phase V is stable up to the highest pressure attained (55.4 GPa). During the decompression process, Phase V was retained at 8.6 GPa, Phase IV and V coexisted at 3.5 GPa, and Phase II was recovered when pressure was released back to ambient condition. The phase transition pressures are summarized in Table I, and the representative diffraction patterns are shown in Fig. 2A.

The Bragg peak positions were determined by the program Peakfit v4.11 (Systat Software Inc.). At ambient condition, 12 peaks were resolved and indexed to the tetragonal structure with $I4/mcm$ symmetry (Phase II). The cell parameters obtained at ambient condition, $a = b = 6.545 \pm 0.001$ and $c = 8.103 \pm 0.002$, are in excellent agreement with the results in the literature²⁸. In the investigation of the unknown structure of each high-pressure phase, the crystal system and unit cell were yielded by indexing the Bragg peaks using the program Dicvol04³³, the number of formula units per unit cell (“Z” number) was calculated from volume decrements, and the space group was

determined by the systematic extinctions listed in the international tables for crystallography (Volume A)³⁴. For Phase III, indexing using Dicvol04 yielded a unique solution, which led to a unit cell in monoclinic symmetry with $Z = 4$. In its diffraction pattern, a systematic extinction of (hkl) with $h+k$ odd was observed so the possible space groups of Phase III are $C2$, Cm , and $C2/m$. Since the ambient CsN_3 (tetragonal Phase II) belongs to the point group of $4/mmm$, its high pressure form (monoclinic Phase III) is more probable in the point group of $2/m$ than 2 or m (the degrade of symmetry element from 4-fold axis to 2-fold axis, and the loss of mirror planes can be ascribed to the distortion of the unit cell from tetragonal to monoclinic). Moreover, among all the known structures of alkali azides (including the phases at non-ambient conditions), there exist two monoclinic structures (LiN_3 and $\alpha-NaN_3$), and both of them belong to $C2/m$ space group¹⁰. Therefore, the space group of CsN_3 Phase III is assigned as $C2/m$. For Phase IV, its crystal system is determined as monoclinic, because all of the indexing solutions led to the monoclinic symmetry. The most probable index yielded a unit cell with $Z = 8$. A systematic extinction was observed, $(0k0)$ with k odd, therefore the space group of Phase IV is determined as $P2_1/m$ or $P2_1$ (both of them have the same systematic extinction due to symmetry). For Phase V, its crystal system is determined as triclinic, because all of the indexing solutions led to a triclinic symmetry. The most probable index yielded a unit cell with $Z = 12$. The space group of Phase V is determined as $P1$ or $P\bar{1}$, because they are the only possible space groups in triclinic symmetry and neither of them has a systematic extinction. The indexing of Phase III, IV and V are shown in Fig. 2B.

To investigate the atomic fractional coordinates of Phase III, the diffraction pattern obtained at 2.9 GPa in NSLS was refined using Rietveld method with the FullProf

software³⁵. To construct the original structure for the refinement, an investigation of all the known structures of alkali azides were performed, and it is found that all of them have linear azide anions, with either parallel or perpendicular arrangements to each other^{10, 36} (which can be understood by the fact that the parallel or perpendicular arrangement is energetic favorable). Moreover, it is also observed that in all the structures with an orthogonal unit cell ($a \perp b \perp c$), the azide chains are perpendicular to each other (as seen in KN_3 , $\alpha\text{-RbN}_3$, and CsN_3 (Phase II)³⁶); and in all the structures with a non-orthogonal unit cell, the azide chains are parallel (as seen in LiN_3 , $\alpha\text{-NaN}_3$, and $\beta\text{-NaN}_3$ ^{10, 36}). Since CsN_3 Phase III has a non-orthogonal unit cell, a parallel chain structure for the azide anions was applied in the refinement. Because the II-III phase transformation happens at a relative low pressure (0.5 GPa), it is reasonable to assume the atoms in Phase III reside on the positions similar to that of Phase II. Therefore, the Wyckoff positions of Cs and four N atoms were assigned to be $4i$, $2b$, $2d$, $4i$, $4i$, respectively (as seen in Table II). The mean quality factors of the refinement are $R_p = 6.19\%$, $R_{wp} = 8.24\%$, $\chi^2 = 1.47$, and the Rietveld plot is shown in Fig. 3. The resulted atomic fractional coordinates are summarized in Table II and plotted in Fig. 4. The results indicate that the azide anion chains $\text{N}_4\text{-N}_1\text{-N}_4$ and $\text{N}_3\text{-N}_2\text{-N}_3$ reside on two crystallographically nonequivalent sites, which is in agreement with the results from the previous Raman study¹². The result shows that CsN_3 keeps its layered structure; and the orientation of azide anions rotates obviously during the II-III transition. Unlike lying in the ab plane in Phase II, the azide anions tilt up slightly through an angle of 3.85° in Phase III. The tilts of azide anions may be ascribed to the shear of layers, which phenomenon is also seen in LiN_3 ²⁶ and NaN_3 ¹⁰. The atomic fractional coordinates of Cs deviates slightly from their values in Phase II. In

Phase II, the Cs atom resides on special Wyckoff position $4a$ at $(0, 0, 0.25)$; while in Phase III, it resides on general Wyckoff position $4i$ at $(-0.0196 \pm 0.0007, 0, 0.2745 \pm 0.0005)$. It is of note that the sum of the ionic radii of Cs and N is 3.32 \AA^{28} under ambient condition. If we assume the shrink of ionic radii is proportional to the shrink of the unit cell volume, the sum of ionic radii of Cs and N will become 2.88 \AA at 2.9 GPa, which is 8% bigger than the shortest distance between Cs and N yielded in the refinement (2.67 \AA). Thus we do not exclude the possibility that cesium forms some degree of covalent bonding with the azide group under high pressure. It should be pointed out that the atomic fractional coordinates of N_3 and N_4 resulted from the fitting may not be accurate because of the large difference in the scattering ability of Cs and N, and the non-perfect fitting (as shown in Fig. 3, the difference between the observed and calculated patterns) due to the preferred orientation in the sample; nevertheless, the trend of change during the phase transition should be reliable.

To reveal the compressibility of each phase, the cell parameters and volume per formula unit were computed from the peak positions measured at varying pressures³⁷. The change of cell parameters are illustrated in Fig. 5 and 6. For Phase II, the compressibility of c direction has little difference with that of a direction when one takes into account the experimental errors (Fig. 5B), which contrasts with the observation that the Cs-Cs distances in the c direction are much shorter than those in the $[1\ 1\ 0]$ directions (4.045 and 4.625 \AA , respectively in Phase II under ambient condition²⁸). This implies that the repulsions between azide anions dominate the compressibility behavior of Phase II. For Phase III, the smallest deformation occurs along the a axis, and the deformation along the b and c axis are equivalent (Fig. 5C). The monoclinic angle β of Phase III

increases under compression (a linear fitting of the P - β data of Phase III yields a slope of $0.16 \pm 0.02^\circ \text{ GPa}^{-1}$, as shown in Fig. 6). This interlayer shear may imply a tilt of the azide anions during the compression, which phenomenon was also observed in the high pressure behavior of LiN_3 ²⁶. For Phase IV, its compressibility shows isotropy in all three directions a , b , and c (Fig. 5D), and the monoclinic angle β shows little change with increasing pressure (a linear fitting of the P - β data of Phase IV yields a slope of $0.012 \pm 0.009^\circ \text{ GPa}^{-1}$, as shown in Fig. 6). The isotropic compressibility and stable monoclinic angle of Phase IV infer that its unit cell keeps the same geometric shape and shrinks uniformly under compression. This may imply that the atomic fractional coordinates of Phase IV have little change with increasing pressure, which infers that the azide anions of Phase IV keep almost the same orientation during compression.

Fig. 7 shows the volume per formula unit as a function of pressure. The volume reduction of Phase II-III transition is 4% from 0.4 GPa to 0.5 GPa in this study, which is in agreement with the study of Pistorius⁹. By fitting the P - V data of each phase to the second-order Birch–Murnaghan Equation of State³⁸, the bulk moduli of Phase II, III, IV, and V were yielded as $18 \pm 4 \text{ GPa}$, $20 \pm 1 \text{ GPa}$, $27 \pm 1 \text{ GPa}$ and $34 \pm 1 \text{ GPa}$, respectively. The increasing bulk moduli infer an enhancement of bond strength during phase transitions.

A comparison of the properties and phase transition pressures of alkali azides are given in Table III to provide insight into the phase transition mechanism. A previous theoretical work reported that the closeness of the internitrogen distances of the alkali azides to the calculated N-N bond length for the free azide ion $\Delta(\text{N-N})$ has the following order for the alkali azides: $\text{LiN}_3 > \alpha\text{-NaN}_3 > \text{KN}_3 > \alpha\text{-RbN}_3 > \text{CsN}_3(\text{Phase II})$ ³⁶. Moreover,

the bond order for the alkali metal-end N bonds decrease in the same order as well³⁶. (The bond order is a measure of the overall bond strength between two atoms. A high value of the bond order indicates a stronger bond with a covalent character, while a low value shows a weaker bond with an ionic nature³⁶). Both of the two facts indicate that their ionic character intensifies in the following sequence: $\text{LiN}_3 < \alpha\text{-NaN}_3 < \text{KN}_3 < \alpha\text{-RbN}_3 < \text{CsN}_3(\text{Phase II})$ ³⁶. On the other hand, it is found that the transition pressures of the alkali azides decrease in the order of: $\text{LiN}_3 > \alpha\text{-NaN}_3 > \text{KN}_3 > \alpha\text{-RbN}_3 > \text{CsN}_3(\text{Phase II})$ ^{9, 14, 26, 39}. Therefore it can be concluded that the ionic character of the compounds plays a key role in the pressure-induced phase transitions of alkali azides (more specifically, the phase transitions are favored by a stronger ionic character of the compounds). This can be understood by the fact that in the alkali azides, all available valencies are bound to azide groups, thus their phase stability is dominated by their ionic character.

IV. SUMMARY AND CONCLUSIONS

High-pressure study of cesium azide (CsN_3) up to 55.4 GPa revealed three phase transitions at 0.5 GPa, 4.4 GPa, and 15.4 GPa, respectively. The space groups for the high-pressure phases are determined as follows: Phase III: $C2/m$; Phase IV: $P2_1/m$ or $P2_1$; and Phase V: $P1$ or $P\bar{1}$. During the II-III phase transition, the layered structure is kept and the azide anions rotate obviously. The compressibility of cell parameters a , b , and c is isotropic in Phase II and IV, while anisotropic in Phase III. The monoclinic angle β of Phase III increases under compression; while the β angle of Phase IV shows little change with increasing pressure. The bulk moduli of Phase II, III, IV, and V are determined to be

18 ± 4 GPa, 20 ± 1 GPa, 27 ± 1 GPa and 34 ± 1 GPa, respectively. The ionic character of alkali azides plays a key role in their pressure-induced phase transitions.

ACKNOWLEDGEMENTS

Thanks are due to Dr. Zhongwu Wang for his technical assistance. This work was supported by the Defense Threat Reduction Agency (HDTRA1-09-0034), the Army Research Office (W911NF-09-1-0001), and the National Science Foundation (DMR-0619215).

REFERENCES

- 1 B. L. Evans and A. D. Yoffe, Proc. R. Soc. London, Ser. A **238**, 568 (1957).
2 B. L. Evans, A. D. Yoffe, and P. Gray, Chem. Rev. (Washington, DC, U. S.) **59**,
3 515 (1959).
4 I. Agrell, Acta Chem. Scand. **25**, 2965 (1971).
5 C. M. Pereira and M. M. Chaudhri, Journal of Energetic Materials **7**, 297 (1989).
6 B. P. Aduiev, E. D. Aluker, G. M. Belokurov, Y. A. Zakharov, and A. G.
7 Krechetov, J. Exp. Theor. Phys. **89**, 906 (1999).
8 S. K. Deb, B. L. Evans, and A. D. Yoffe, Symp. (Int.) Combust., [Proc.], 829
9 (1962).
10 C. E. Weir, S. Block, and G. J. Piermarini, J. Chem. Phys. **53**, 4265 (1970).
11 J. Liu, C. g. Duan, M. M. Ossowski, W. N. Mei, R. W. Smith, and J. R. Hardy,
12 Mater. Res. Bull. **36**, 2035 (2001).
13 C. W. F. T. Pistorius, J. Chem. Phys. **51**, 2604 (1969).
14 G. E. Pringle and D. E. Noakes, Acta Crystallogr., Sect. B **24**, 262 (1968).
15 H. J. Mueller and J. A. Joebstl, Z. Kristallogr., Kristallgeom., Kristallphys.,
16 Kristallchem. **121**, 385 (1965).
17 Z. Iqbal and C. W. Christoe, J. Chem. Phys. **62**, 3246 (1975).
18 F. J. Owens, J. Phys. C **12**, 2255 (1979).
19 M. I. Eremets, M. Y. Popov, I. A. Trojan, V. N. Denisov, R. Boehler, and R. J.
20 Hemley, J. Chem. Phys. **120**, 10618 (2004).
21 M. Popov, Phys. Lett. A **334**, 317 (2005).
22 Z. Iqbal and C. W. Christoe, Solid State Commun. **17**, 71 (1975).
23 S. R. Aghdaee and A. I. M. Rae, Acta Crystallogr., Sect. B: Struct. Sci. **B40**, 214
24 (1984).
25 G. J. Simonis and C. E. Hathaway, Phys. Rev. B **10**, 4419 (1974).
26 L. B. Kanney, N. S. Gillis, and J. C. Raich, J. Chem. Phys. **67**, 81 (1977).
27 Z. Iqbal, J. Chem. Phys. **59**, 1769 (1973).
28 A. K. McMahan and R. LeSar, Phys. Rev. Lett. **54**, 1929 (1985).
29 A. F. Goncharov, E. Gregoryanz, H.-k. Mao, Z. Liu, and R. J. Hemley, Phys. Rev.
30 Lett. **85**, 1262 (2000).
M. I. Eremets, R. J. Hemley, H.-k. Mao, and E. Gregoryanz, Nature (London, U.
K.) **411**, 170 (2001).
M. I. Eremets, A. G. Gavriiliuk, I. A. Trojan, D. A. Dzivenko, and R. Boehler, Nat.
Mater. **3**, 558 (2004).
M. I. Eremets, A. G. Gavriiliuk, and I. A. Trojan, Appl. Phys. Lett. **90**, 171904/1
(2007).
S. A. Medvedev, I. A. Trojan, M. I. Eremets, T. Palasyuk, T. M. Klapoetke, and J.
Evers, J. Phys.: Condens. Matter **21**, 195404/1 (2009).
S. M. Peiris and T. P. Russell, J. Phys. Chem. A **107**, 944 (2003).
U. Mueller, Z. Anorg. Allg. Chem. **392**, 159 (1972).
H. K. Mao, P. M. Bell, J. W. Shaner, and D. J. Steinberg, J. Appl. Phys. **49**, 3276
(1978).
H. K. Mao, J. Xu, and P. M. Bell, J. Geophys. Res., B **91**, 4673 (1986).

- 31 A. P. Hammersley, S. O. Svensson, M. Hanfland, A. N. Fitch, and D.
Hausermann, *High Press. Res.* **14**, 235 (1996).
- 32 I. L. Spain and D. J. Dunstan, *J. Phys. E: Sci. Instrum.* **22**, 923 (1989).
- 33 A. Boultif and D. Louer, *J. Appl. Crystallogr.* **37**, 724 (2004).
- 34 T. Hahn and Editor, *International Tables for Crystallography; Volume A, Space
Group Symmetry: Fifth, Revised Edition*, 2001).
- 35 J. Rodriguez-Carvajal, *Physica B (Amsterdam)* **192**, 55 (1993).
- 36 W. Zhu, J. Xiao, and H. Xiao, *J. Phys. Chem. B* **110**, 9856 (2006).
- 37 See Supplemental Material at for unit cell parameters and volume per formula
unit at varying pressures.
- 38 F. Birch, *Phys. Rev.* **71**, 809 (1947).
- 39 C. Ji, F. Zhang, D. Hou, H. Zhu, J. Wu, M.-C. Chyu, V. I. Levitas, and Y. Ma, *J.
Phys. Chem. Solids* **72**, 736 (2011).

Table I. Phase Transition Pressures of CsN₃. P_i indicates the initial pressure of phase transition, and P_c indicates the completion pressure.

	II-III	III-IV	IV-V
P _i (GPa)	0.4~0.5	3.8~4.4	15.1~15.4
P _c (GPa)	0.4~0.5	4.4~5.0	23.7~24.7

Table II. Atomic fractional coordinates of Phase III at 2.9 GPa. The Wyck stands for the Wyckoff positions of space group $C2/m$. The number in the parentheses represent the error in the last digit resulted from the refinement.

Atom	Wyck	x	y	z
Cs	$4i$	-0.0196(7)	0	0.2745(5)
N ₁	$2b$	0	0.5	0
N ₂	$2d$	0	0.5	0.5
N ₃	$4i$	0.1716(9)	0.5	0.4914(6)
N ₄	$4i$	0.1716(9)	0.5	-0.0086(6)

Table III. Comparison of properties and phase transition pressures of alkali azides.

alkali azides	$\Delta(\text{N-N})$	metal-end N bond order	phase transition pressures (under room temperature)
LiN_3	0.006^{36}	0.14^{36}	No transitions up to 62 GPa ²⁶
$\alpha\text{-NaN}_3$	0.005^{36}	0.12^{36}	19 GPa ¹⁴
KN_3	0.003^{36}	0.02^{36}	15.5 GPa ³⁹
$\alpha\text{-RbN}_3$	0.002^{36}	0^{36}	0.5 GPa ⁹
$\text{CsN}_3(\text{Phase II})$	0.001^{36}	0^{36}	0.4 GPa ⁹ , 0.4 ~ 0.5 GPa ^{this study}

Figure Captions:

Fig. 1. The crystal structure of Phase II. The Cs atoms are represented by black spheres and N atoms by grey spheres.

Fig. 2. X-ray diffraction patterns of CsN₃ at selected pressures. In Fig. 2A, different phases are shown by the Roman numerals on the right of the patterns. The coexistence of two phases at 4.4 GPa and 15.4 GPa indicates the onset of the phase transitions. The asterisks indicate the appearance of new Bragg peaks due to the phase transitions. The three patterns on the top of the figure (with a letter “d” in the parentheses besides the pressure) demonstrate the decompression process. Fig. 2B shows the miller indices of the high-pressure phases.

Fig. 3. Rietveld refinement patterns for Phase III at 2.9 GPa. The observed diffraction intensities are represented by the dots, and the calculated pattern by the solid line. The solid curve at the bottom represents the difference between the observed and calculated intensities. Short vertical bars below the observed and calculated patterns indicate the positions of allowed Bragg reflections.

Fig. 4. The crystal structure of Phase III yielded from the refinement at 2.9 GPa. The Cs atoms are represented by black spheres and N atoms by grey spheres.

Fig. 5. The pressure dependence of the cell parameters *a*, *b*, and *c* of CsN₃.

Fig. 6. The pressure dependence of the monoclinic angle β of Phase III and IV. The solid lines demonstrate the linear fitting of the P- β data.

Fig. 7. Volume per formula unit change of CsN₃ with pressure. The solid lines demonstrate the fitting of the P-V data to the second-order Birch-Murnaghan Equation of State.

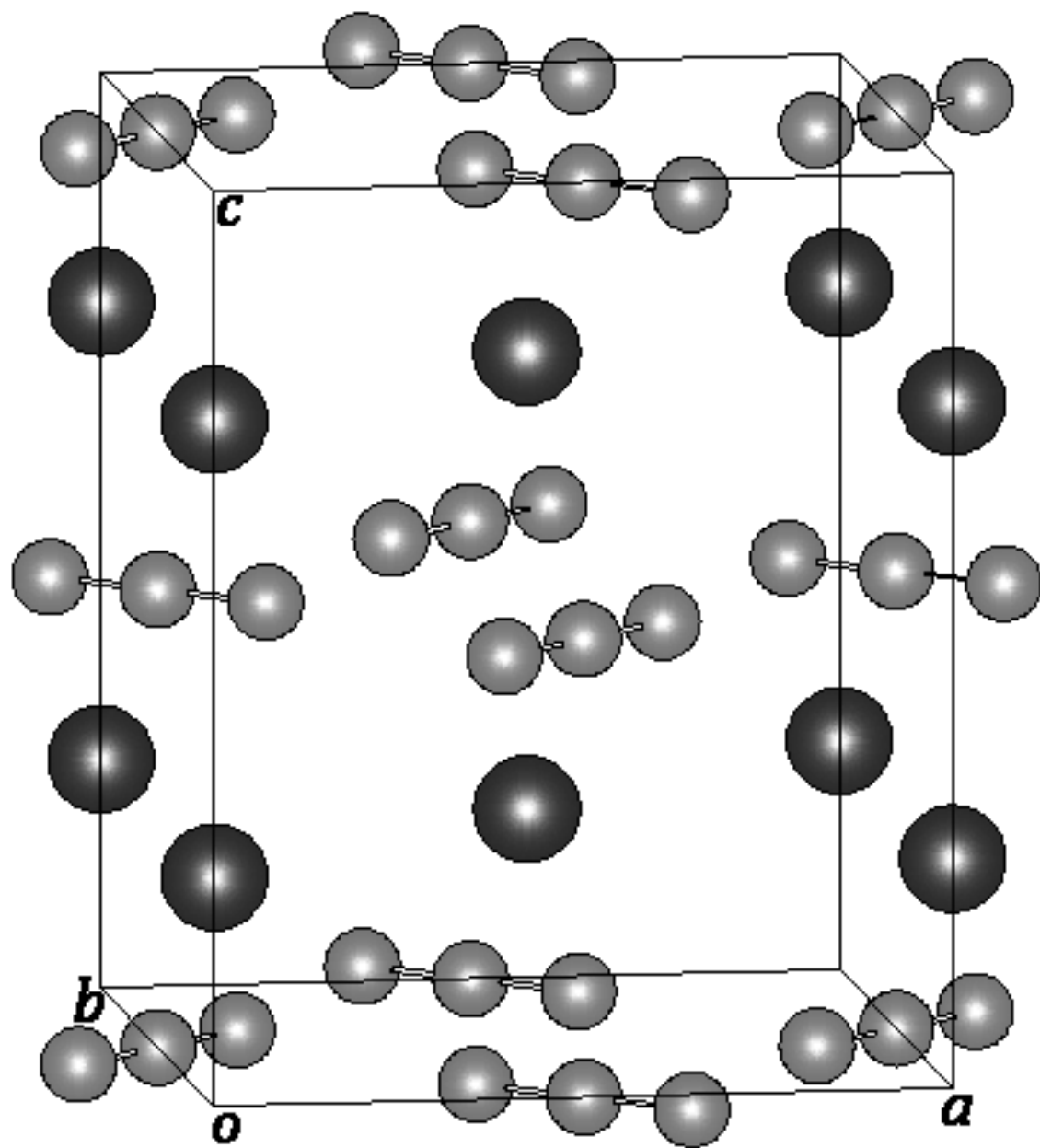


Figure 1

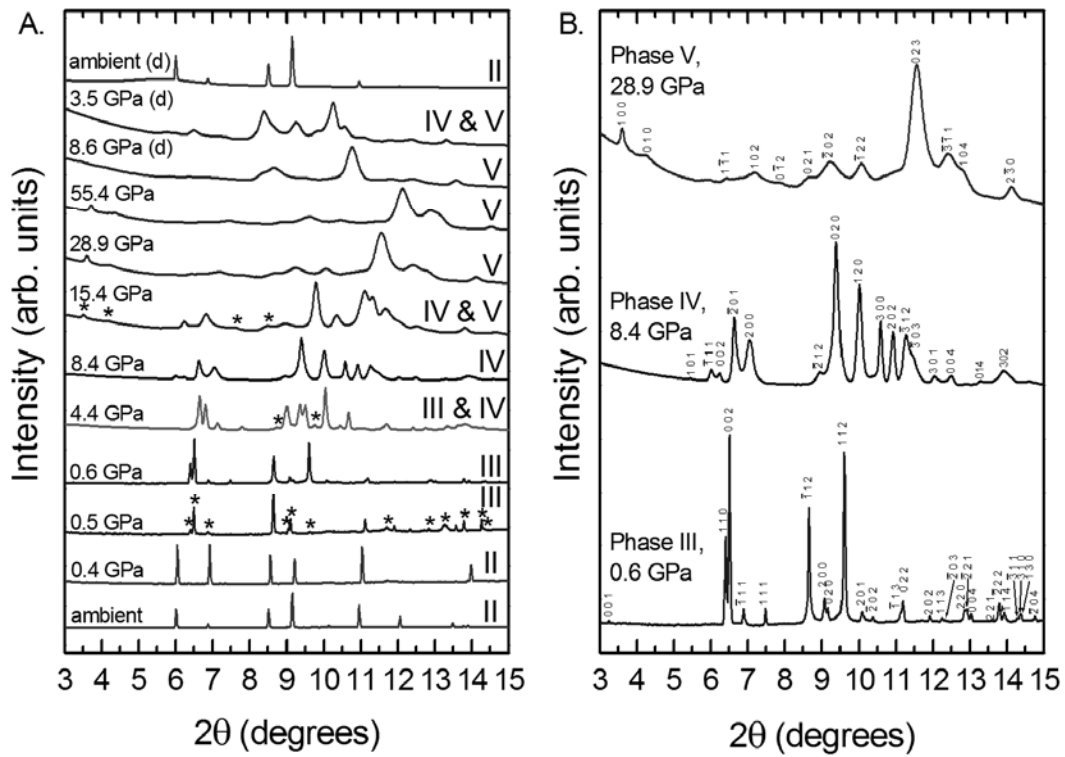


Figure 2

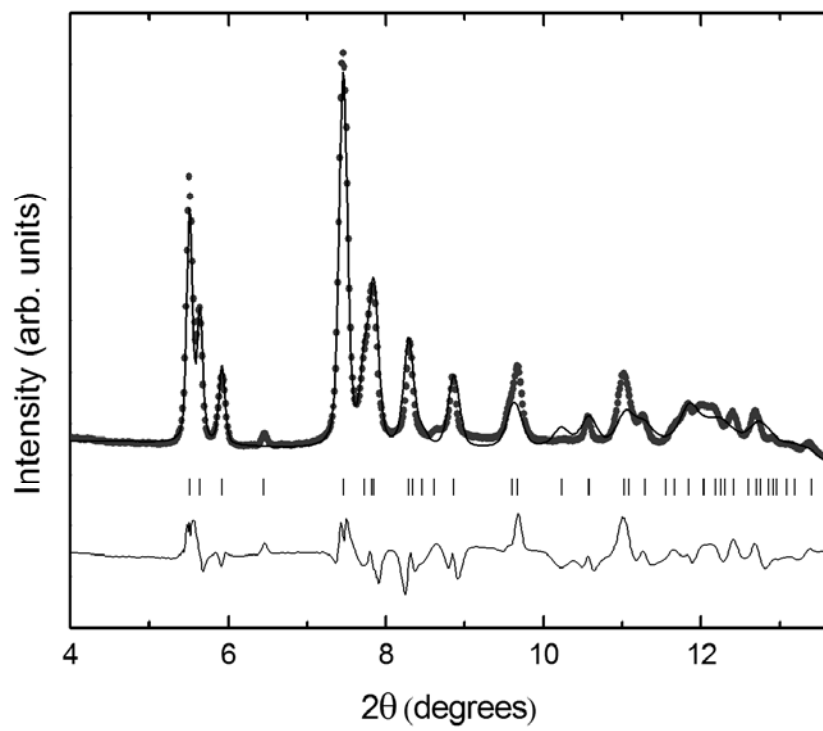


Figure 3

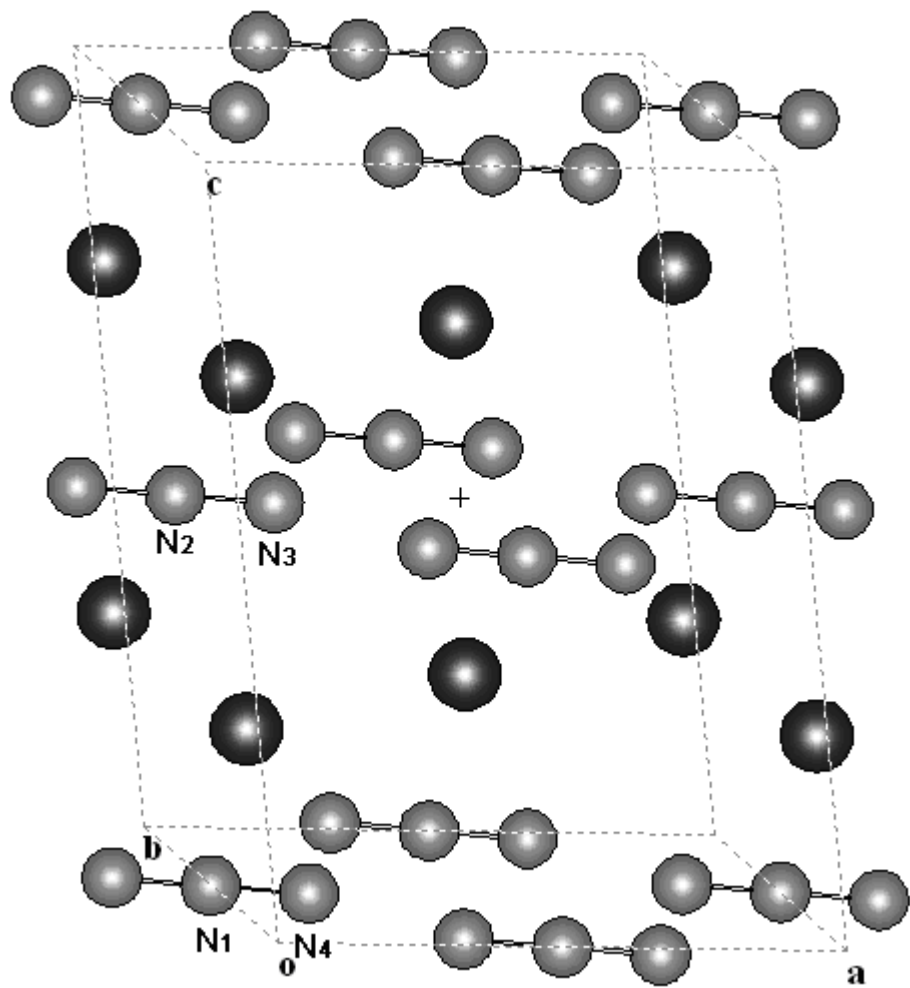


Figure 4

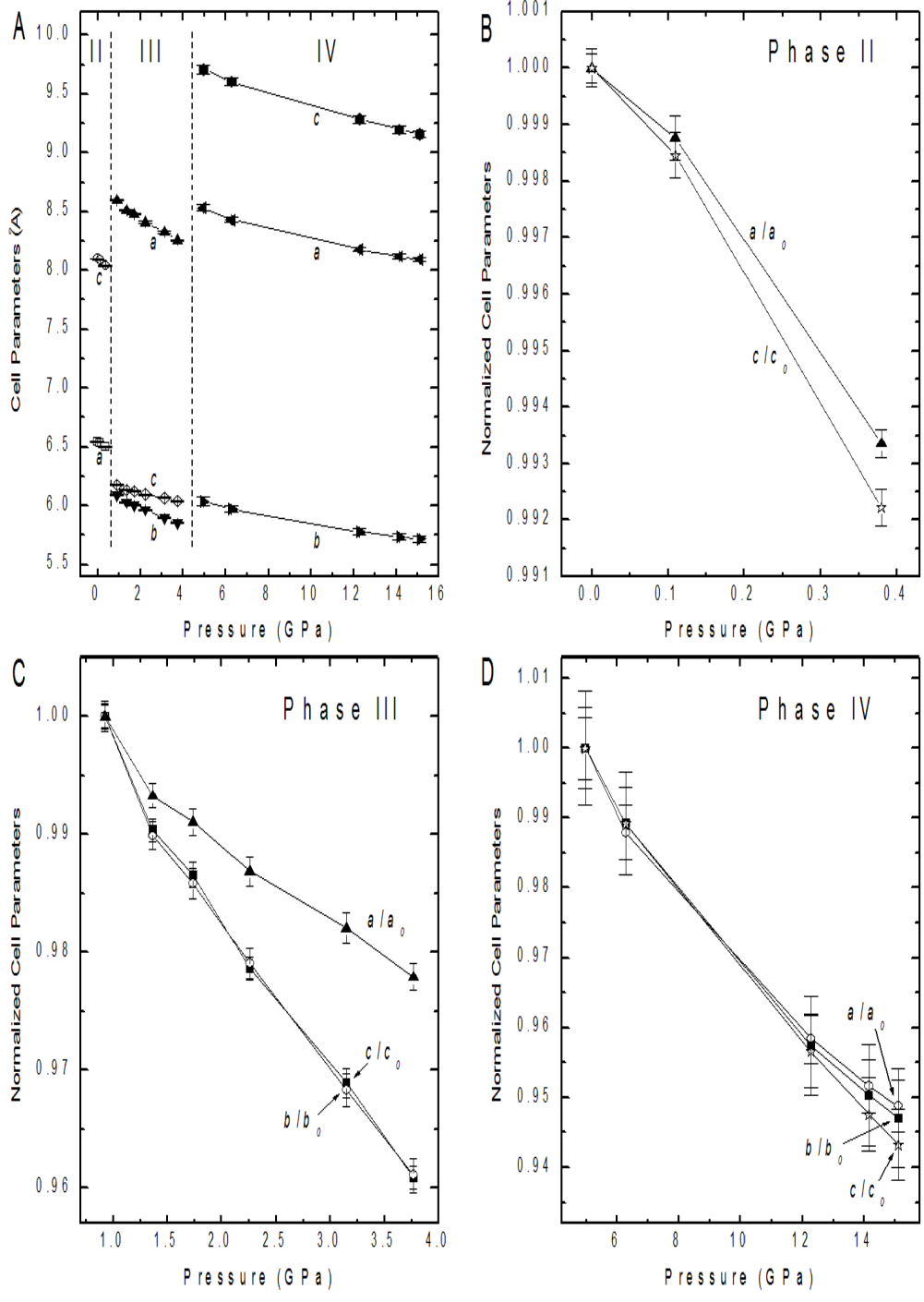


Figure 5

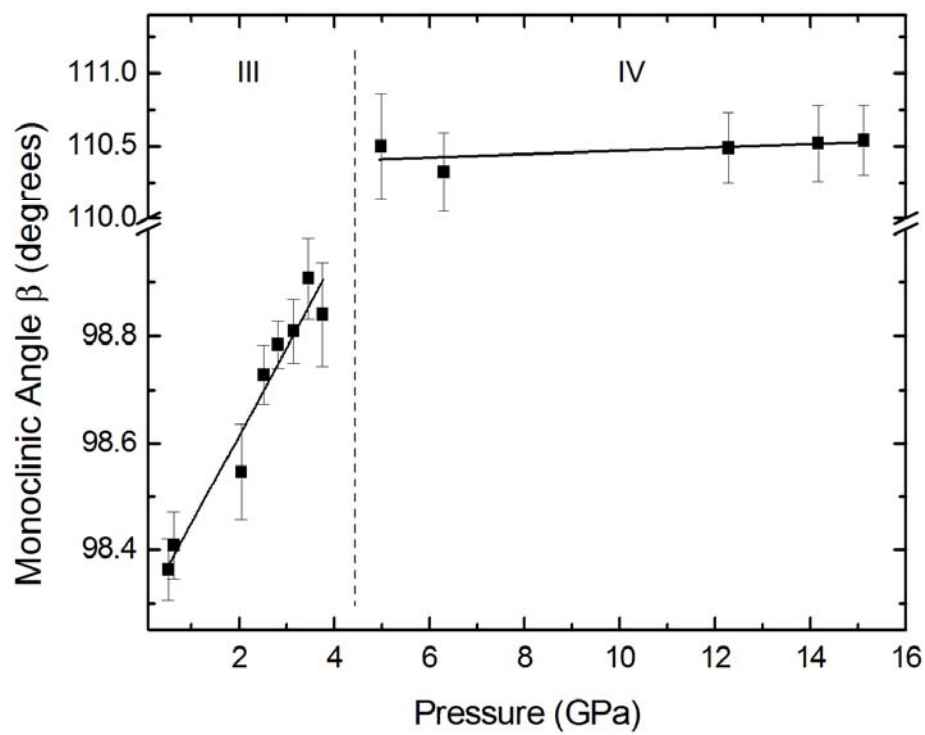


Figure 6

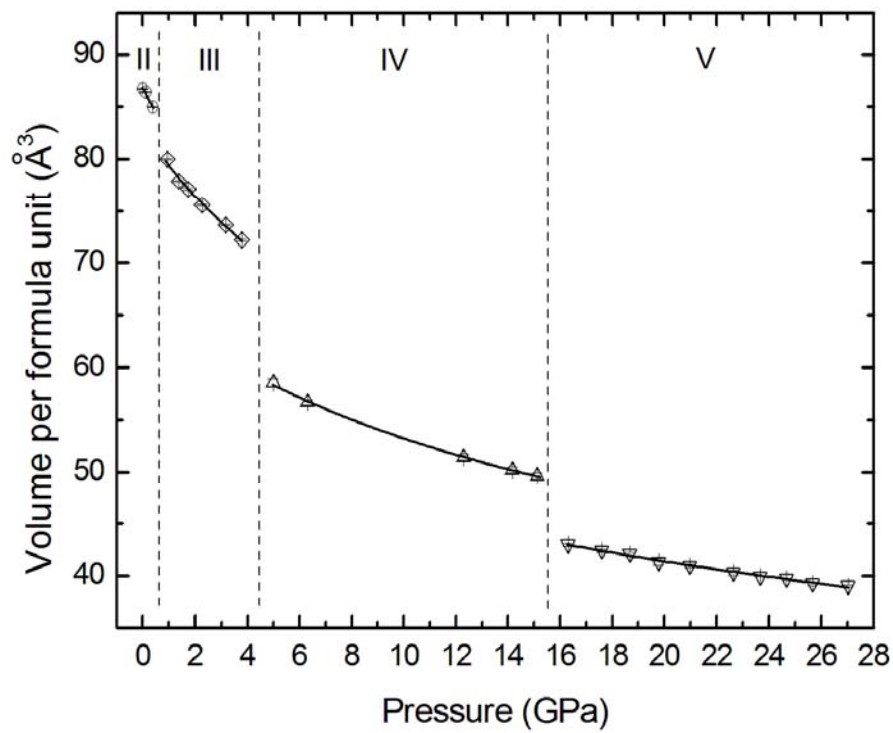


Figure 7